Analog Radio-Frequency Interference (RFI) Suppression System for Microwave Radiometers

P.N. Mohammed *Member, IEEE,* J. K. Knuble *Member, IEEE,* and J. R. Piepmeier *Member, IEEE*

***Abstract*— Microwave radiometers use radio spectrum dedicated to sensing the environment. As wireless communications and other active services proliferate, this allocated spectrum is nearly being crowded out. The potential result is corrupted satellite measurements of the weather, the climate, and the environment. The Analog Radio-Frequency Interference Suppression System (ARFISS) is a combination of detection hardware and algorithms designed to address this problem. By observing the statistics of an incoming signal to a microwave radiometer, it can be determined if the signal is contaminated by radio frequency interference (RFI) which can cause unwanted anomalies in the data. The analog multiplier system is part of ARFISS which can potentially be used to detect and mitigate radio frequency interference (RFI) in conventional radiometers. In addition to measuring statistics of an incoming signal, changes in the video spectrum of the square-law detector can be monitored to detect RFI. This paper will present experimental results to show proof of concept as well as results of the post-detector spectral analysis. This design, which uses purely analog components at radio and/or intermediate frequencies, allows the system to easily augment conventional radiometer architectures used in both airborne and space borne instruments. An equivalent high- speed digital design would add an impractical level of cost and complexity to radiometer designs using today's technology. Thus, the Analog Radio-Frequency Interference Suppression System (ARFISS) is being developed to reduce risk and to enable NASA and the Nation to maintain the impressive legacy of precision Earth observations made using microwave radiometers into the future whilst the radio spectrum becomes evermore utilized.**

***Index Terms*— Radiometer, signal detection, radio-frequency interference, RFI, kurtosis**

I. Introduction

Radio frequency interference can compromise microwave radiometer measurements. Spectrum is allocated for passive remote sensing, however as active services proliferate this spectrum is becoming increasingly vulnerable to interference. Moderate to high levels of RFI can be easily detected using spectral difference methods but low level RFI cannot be easily distinguished from the natural geophysical variability. The Analog Radio-Frequency Interference Suppression System (ARFISS), incorporates a simple RFI detector for use in microwave radiometers.

ARFISS is based on the concept of using the kurtosis statistic to determine if the incoming signal is non-Gaussian RFI. The system was designed to augment existing radiometer architectures using common RF components.

Section II includes a description of the multiplier system; a discussion of the detector linearization and experiments are discussed in Section III followed by a video frequency analysis in Section IV and a discussion in Section V.

The authors are with the Microwave Instruments & Technology Branch at NASA's Goddard Space Flight Center in Greenbelt, Maryland, USA. Mohammed is also with GEST at UMBC.

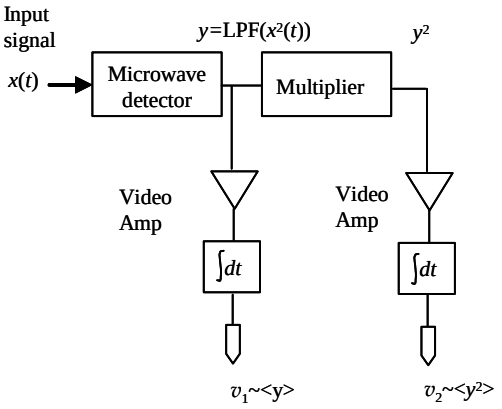

Fig. 1. Block diagram of multiplier system.

II. The Multiplier System

The multiplier system is part of an analog radio frequency interference suppression system that can potentially be used to detect and mitigate RFI in conventional radiometers. The system includes a square-law diode detector for measuring the total power out of the radiometer, followed by a multiplier which acts as a higher-order statistical fourth-moment detector.

The signal power measured by the square-law detector (without interference) consists of naturally occurring thermal emission, including that from the sky, plus thermal noise generated in the radiometric system, all modeled using Gaussian distributions. Gaussian signals have a constant relationship between their power or the second central moment, μ_2, and their fourth central moment, μ_4. The ratio

$$\beta_2 = \frac{\mu_4}{\mu_2^2} \tag{1}$$

is called the kurtosis and is equal to three if the input is Gaussian [1]. The deviation of this quotient from its constant value of three is an indicator of the presence of non-Gaussian RFI. Since the kurtosis is dependent on the statistical properties of the measured signals, low level RFI that would be undetected by conventional methods would be easily identified.

The multiplier system approximates the true kurtosis β_2,

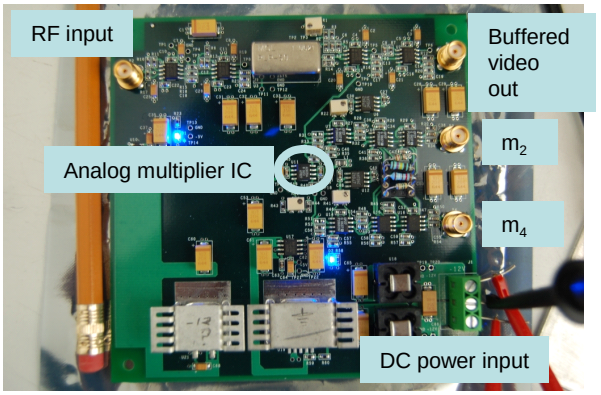

Fig. 2. Photograph of multiplier hardware.

and is defined as

$$\alpha \equiv \frac{\langle y^2 \rangle}{\langle y \rangle^2}, \tag{2}$$

where $y(t)$ is the baseband video signal of the detected RF $x(t)$. The operator $\langle \cdot \rangle$ denotes the expected value.

A block diagram of the system used to approximate the kurtosis is shown in Fig. 1 and a photograph of the hardware is shown in Fig. 2. The microwave detector measures the second central moment, y, and the multiplier measures the fourth central moment, y^2. The incoming signal $x(t)$ is centered at the RF or IF frequency depending if the radiometer uses direct detection or down conversion. The output $y(t)$ is a baseband video frequency (VF) signal where $y(t) = LPF(x^2(t))$, which is the low pass filtered output of the first detector. The multiplier squares $y(t)$ and the video amplifiers produce the two output voltages, v_1 and v_2 which are substituted into (2) to give α.

A. Pseudo Kurtosis with a Gaussian Input

As with the true kurtosis, α is constant as the power of $x(t)$ varies. When $x(t)$ is Gaussian, then

$$\alpha = 2 \tag{3}$$

and the standard deviation of α is

$$\mathrm{NE}\Delta\alpha = \sqrt{\frac{2}{B\tau_v}} \tag{4}$$

where B is the bandwidth of the input and τ_v is the integration time of the video amplifiers.

III. Experiments

A. Linearization

The diode detector and multiplier are inherently nonlinear, thus their nonlinearities must be characterized and removed before the α can be calculated and used as a measure for RFI detection. For the results in this paper a polynomial expansion sufficiently describes these nonlinearities and a linearized α is presented for experimental data.

A constant deflection method [2] is used to obtain the coefficients of the polynomial expansion for the first detector. This is done by observing the noise diode deflections as the antenna noise temperature changes. In a linear system these deflections, which are proportional to system gains, should be constant. Therefore the ratio of any two deflections should be unity where the ratio, D, is defined as

$$D = \frac{v_{a_i} - v_{an_i}}{v_{a_o} - v_{an_o}}. \tag{5}$$

The 0 and i subscripts are the reference and i^{th} measurements respectively; the detector voltages v_{a_i},v_{a_o} are measured while looking through the antenna and v_{an_i},v_{an_o} are detector voltages for the antenna plus noise diode state. Any combination of antenna (v_a) and antenna plus noise diode (v_{an}) values can be used to compute the ratios of noise diode deflections. For ease of calculation the denominator is fixed while v_{a_i} and v_{an_i} are varied. The data used in (5) should be interference free. A system of linear equations is set up by substituting the linearizing formula

$$v_{lin} = v_1 + C_2 v_1^2 + ... \tag{6}$$

into (5). The value v_{lin} is the corrected or linearized voltage and v_1 is the measured detector voltage output of the first detector minus the dc offset added by the video amplifier as indicated in Fig. 1. D is computed for several values of v_{a_i} and v_{an_i}, equated to one and the unknown coefficients are obtained by least squares solution. Depending on the dynamic range of the system the second moment detector can be characterized by a second or third order polynomial and a higher order polynomial is used to model the multiplier. This method is advantageous since the system used to measure the second central moment is linearized rather than just the detector.

Forward models are then used to derive theoretical second and fourth order moments and thus a nonlinear α. The nonlinear α is represented as

$$\alpha_{nonlin} = \frac{d_1 \langle z^2 \rangle + d_2 \langle z \rangle + d_3 \langle z^3 \rangle + ...}{\langle z \rangle^2} \tag{7}$$

where z replaces y in Fig. 1 and the numerator is the nonlinear model for the multiplier. This reduces to a function of v_{lin} and C_2, given by

$$\begin{aligned} \alpha_{nonlin} \quad = \quad & \frac{v_2}{v_1^2} = d_1 \left(2 + f_1 \left(v_{lin}, C_2\right)\right) + \\ & d_2 f_2 \left(v_{lin}, C_2\right) + d_3 f_3 \left(v_{lin}, C_2\right) + ..., \end{aligned} \tag{8}$$

with the only unknowns being d_i (i = 1,2,3...) which include the system gain, d_1. Antenna-look data is substituted into (8) and the remaining unknown instrumental constants are obtained by least squares solution. The antenna-look data is used to calculate instrumental constants since that data set represents the dynamic range of the system. The linearized α is therefore

$$\alpha_{lin} = \frac{\left(\frac{v_2}{v_1^2}\right) - d_2 f_2 - d_3 f_3 - ...}{d_1} - f_1 \tag{9}$$

which should reduce to a value of two for RFI free data. All linearization constants can be estimated once and remain

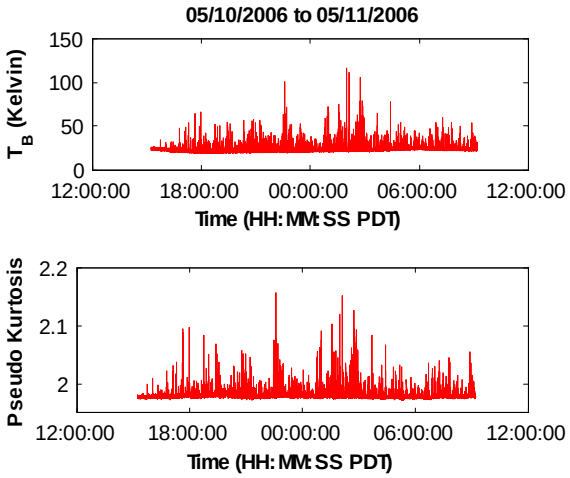

Fig. 3. Typical night long time series.

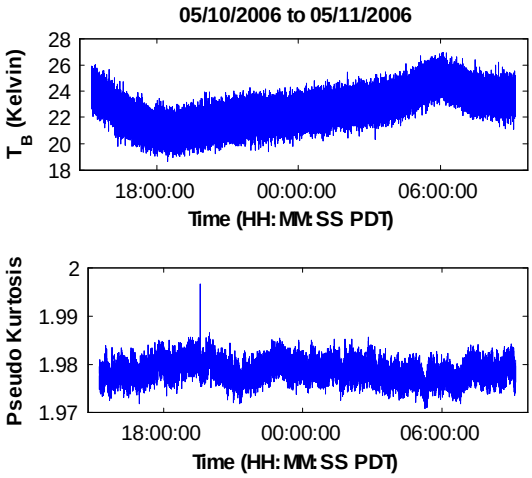

Fig. 4. Night long time series after pulse blanking was applied.

valid provided the system operating point, such as physical temperature, remains constant.

B. PALS

The multiplier system was interfaced with the Passive Active L-band Sensor (PALS) at the Jet Propulsion Laboratory to collect field data over the course of two weeks in April and May 2006. This afforded the opportunity to test the RFI detection system since PALS detects mainly pulsed RFI from nearby airport radars. Data was recorded at 500 kSps and later linearized, calibrated and reduced to 0.5 second integration time series of brightness temperature T_B and pseudo kurtosis, α. A typical night long time series from (05/10/2006 to 05/11/2006) is shown in Fig. 3 and Fig. 4 shows the same data after a conventional pulse blanking technique was applied. In Fig. 4, it is evident that the pulse blanking did not remove all the RFI as there is a noticeable spike at around 19:35 PDT in the pseudo-kurtosis time series. The peak in antenna brightness temperature at around 6 am PDT corresponds to the galactic plane crossing. This increase in radiation from the sky is due to hydrogen line emission concentrated in the plane of the galaxy. See [3] for more details on galactic noise and its effects on passive remote sensing.

The linearization process described in Section III A was applied to all 0.5 second integrated data. Data was collected to obtain linearization constants by slowly sliding a microwave absorber over the aperture of the PALS antenna. This varied the T_B from cold sky to ambient black body thereby producing a wide range of power levels needed to accurately characterize the detectors.

A conventional pulse detection and blanking algorithm similar to that used in [4], was also applied to all PALS data. For each 0.5 second window, a threshold level is set and samples greater than that limit are removed with the remainder being integrated. The threshold for each window is determined by its mean and standard deviation without the largest 10% of samples, resulting in a detection when

$$y(t) - m(t) \geqslant \beta\sigma(t). \tag{10}$$

The samples are $y(t)$, $m(t)$ is the mean, $\sigma(t)$ is the standard deviation and β is a user defined value that sets the false alarm rate (FAR). In this case $\beta = 7$ minimizes the FAR and allows detection of the majority of pulses.

IV. Video Frequency Analysis

The method of RFI detection discussed in the previous sections uses the kurtosis statistic and results are presented in the time domain. Observations in the frequency domain can also provide useful information for detecting RFI. The RF spectrum of noise with a 20 MHz passband centered at 200 MHz plus a -6 dB INR, AM signal at 215 MHz with 5 MHz sidebands is shown in Fig. 5. The blue line is the noise only spectrum and the yellow line is that of the noise plus interferer. In this lab example, changes to the shape of the RF spectrum is evident when the interferer is introduced. A power spectral density estimate of the passband can therefore allow blanking of the interfered spectrum with the residual integrated spectrum providing an RFI free measurement. However, the frequency down conversion that is necessary to observe this spectrum is not present in direct detection radiometers.

The multiplier system described above can be used to obtain spectral information from the passband without frequency conversion thus enabling spectrum analysis with conventional radiometer architectures. The spectrum output from the square-law detector or the baseband video frequency signal, is the auto-convolution of the input microwave passband. Changes to the shape of the video spectrum with RFI as demonstrated by the lab example in Fig. 6, can be monitored for RFI detection. The interferer is the same as in Fig. 5. The conditions are exaggerated in this illustration as the spectrum is not normalized by its DC value.

Investigation of the video spectrum is further motivated by the fourth and second central moments used to estimate the kurtosis. The fourth central moment is the integrated power spectrum of the video output while the second central moment is the DC value. For the multiplier system, this can

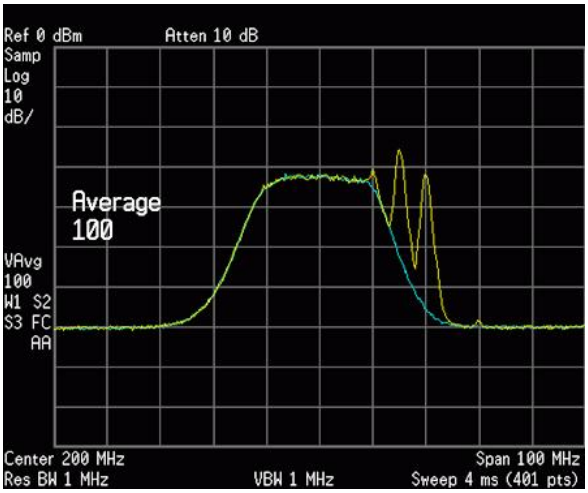

Fig. 5. RF spectrum showing noise only (blue) and noise plus interferer (yello).

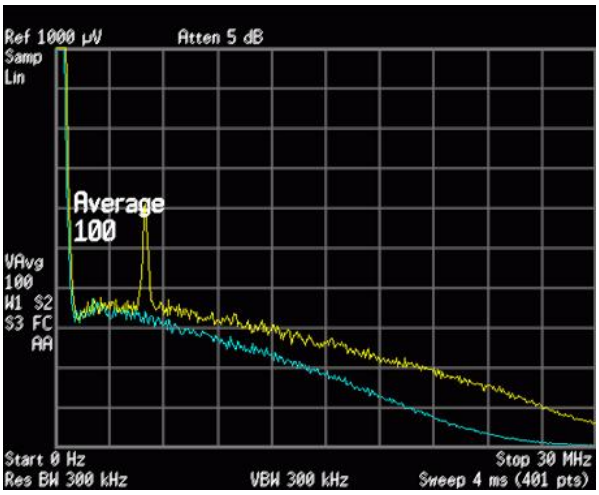

Fig. 6. Video frequency spectrum of noise (blue) and noise plus interferer (yellow).

be expressed mathematically as

$$m_4 = E\left\{V_v^2(t)\right\} = \int_0^f S_v(f)df \tag{11}$$

and

$$m_2 = E\left\{V_v(t)\right\} = S_v^{\frac{1}{2}}(0). \tag{12}$$

The kurtosis does not contain video spectrum information, however, additional information available in the video spectrum can possibly be exploited to improve RFI detection.

A. Simulations

A video spectrum analysis (VSA) model was created to investigate changes in the video spectrum to different types of interferers at varying positions in the passband. In this section, the interferer is a CW input.

The passband process was simulated at baseband in order to reduce the sampling rate and thus the number of computations

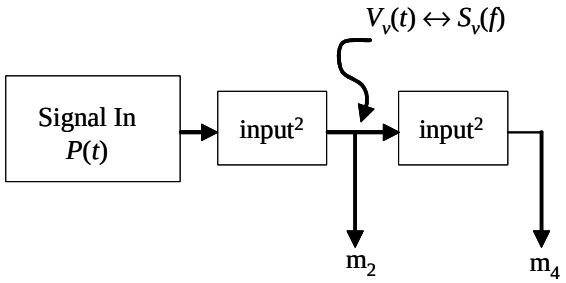

Fig. 7. Block diagram of system.

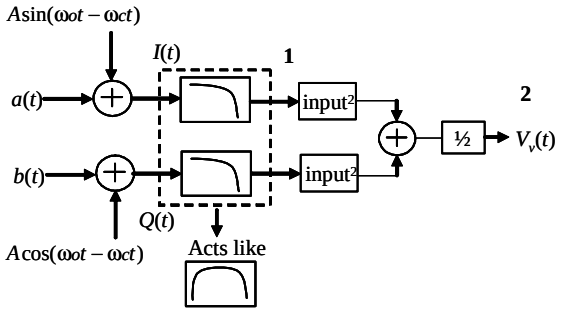

Fig. 8. Block diagram of simulation process.

necessary to obtain a result. The noise plus CW interferer in the passband can be represented as

$$\begin{aligned} P(t) &= a(t)\cos(\omega_o t) + b(t)\sin(\omega_o t) + A\cos(\omega_c t) \\ &= I(t)\cos(\omega_o t) + Q(t)\sin(\omega_o t) \end{aligned} \tag{13}$$

where $a(t)$, $b(t)$, $I(t)$, $Q(t)$ are low pass processes and $A\cos(\omega_c t)$ is the interferer. The I-Q components of $P(t)$ are

$$I(t) = a(t) + A\cos(\omega_o t - \omega_c t) \tag{14}$$

$$Q(t) = b(t) + A\sin(\omega_o t - \omega_c t). \tag{15}$$

The baseband video signal after detection therefore becomes

$$V_v(t) = LPF(P^2(t)) = \frac{1}{2}\left(I(t)^2 + Q(t)^2\right) \tag{16}$$

where $V_v(t)$ is the low pass filtered output of $P^2(t)$ shown in Fig. 7. In order to obtain the output $V_v(t)$, $I(t)$ and $Q(t)$ are simulated then low pass filtered separately and inserted into (16). The frequency content of $V_v(t)$ can then be observed. The block diagram in Fig. 8 shows the simulation process.

In Fig. 8 the power spectral densities at points 1 and 2 are shown in Fig. 9 and Fig. 10 respectively. Both low pass filtered $I(t)$ and $Q(t)$ have the power spectral density shape shown in Fig. 9, where the interferer in the passband is evident. In this example the interferer is at 12.5 MHz from the band center with an INR of 0.5 dB. The low pass filter used in the simulations presented in this paper has 9 poles with 30 MHz of passband.

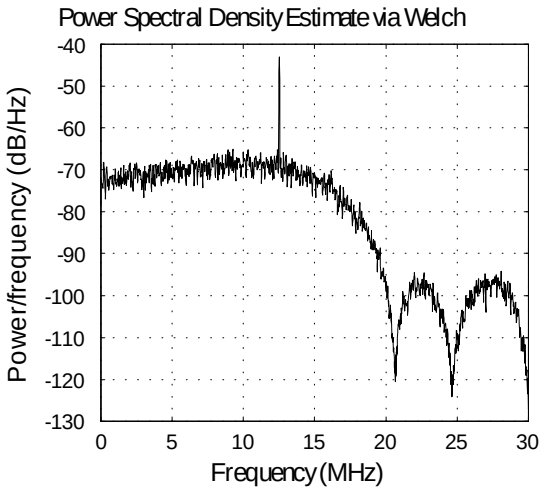

Fig. 9. Low pass filter spectral density.

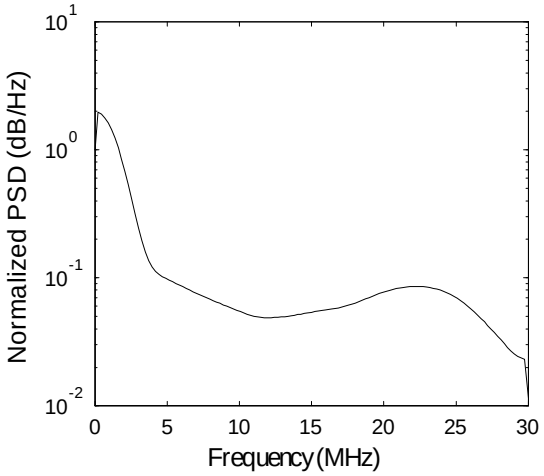

Fig. 10. Video frequency spectral density.

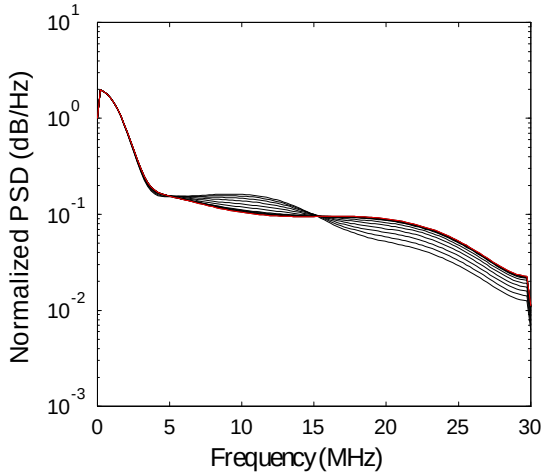

Fig. 11. Power spectral density for different INRs. The interferer is placed at the band center.

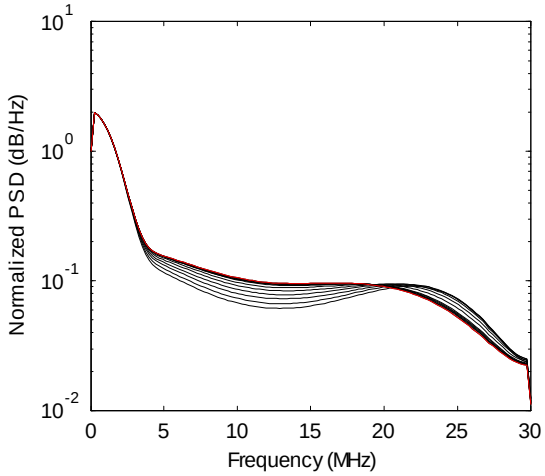

Fig. 12. Power spectral density for different INRs. The interferer is placed at 12.5 MHz from the band center.

B. Results

The video spectrum was observed as the interferer was placed at different points in the pass band. The power spectral density (PSD) of the output are shown for two examples. In Fig. 11, the interferer is placed at the band center and in Fig. 12 the interferer is at 12.5 MHz from the band center. Both plots show the PSDs for INRs ranging from about -22 to -1 dB with the red line indicating a noise only spectrum. Depending on the position of the interferer, the tail of the spectrum either elevates or depresses with increasing INR. It is therefore necessary to further study how the slope of the PSD correlates to the position of the interferer in the spectrum.

V. Conclusions

The performance of the multiplier system in the presence of pulsed RFI was demonstrated with field data collected from a ground based radiometer. The pseudo-kurtosis showed sensitivity to high level RFI as well as RFI that was undetected by conventional pulse blanking techniques. Also presented were some preliminary results of a video spectrum analysis. Since the shape of the spectrum changes with the position of the interferer, this could possibly be used as a measure for RFI detection.

References

[1] A. Papoulis, *Probability Random Variables, and Stochastic Processes, 3rd ed*. New York: McGraw-Hill, pp. 109-111, 1991.

[2] W. J. Wilson, A. B. Tanner, F. A. Pellerano and K. A. Horgan, "Ultra stable microwave radiometers for future sea surface salinity missions," *Instrument Incubator Program Final Report*, JPL Report D-31794 April 2005.

[3] D. M. LeVine and S. Abraham, "Galactic noise and passive microwave remote sensing from space at L-band," *IEEE Trans. Geosci. Remote Sensing*, vol. 42, pp. 119-129 Jan. 2004.

[4] S. W. Ellingson and G. A. Hampson, "Mitigation of radar interference in L-band radio astronomy," *Astrophysical J. Supp. Ser*., 147(1):167-176 July 2003.